Experimental and numerical study of historic masonry with bed joint reinforced repointing

Drougkas, A.; Licciardello, L.; Rots, J.G.; Esposito, R.

DOI
10.47964/1120.9344.19379

Publication date
2020

Document Version
Final published version

Published in
EURODYN 2020 XI International Conference on Structural Dynamics

EURODYN 2020
XI International Conference on Structural Dynamics
M. Papadrakakis, M. Fragiadakis, C. Papadimitriou (eds.)
Athens, Greece, 23–26 November 2020

EXPERIMENTAL AND NUMERICAL STUDY OF HISTORIC MASONRY WITH BED JOINT REINFORCED REPOINTING

Anastasios Drougkas, Lucia Licciardello, Jan G. Rots and Rita Esposito

Delft University of Technology
Stevinweg 1, 2628 CN Delft, The Netherlands
e-mail: {A.Drougkas, L.Licciardello, J.G.Rots, R.Esposito}@tudelft.nl

Keywords: seismic assessment & strengthening, historic masonry structures, full-scale testing, numerical analysis

Abstract. *Induced seismicity due to gas extraction in the province of Groningen in the Netherlands has a noticeable impact on building structures. Historic masonry structures in the area, which are non-engineered and lacking empirical design features often present in traditionally seismic regions, are especially vulnerable to dynamic loading. Compounding the problem, gas extraction additionally generates soil settlement, which can induce damage to masonry buildings and thus reduce their capacity to bear seismic loads.*

The objective of this paper is the evaluation of the performance of a widely used structural intervention method applied in masonry structures in the Groningen region of the Netherlands. This method, initially developed against soil subsidence damage, consists in the embedment of stainless steel helical bars in repointed bed joints. Additionally, diagonal anchors are placed in drilled holes across existing cracks in the masonry. The increase in induced seismicity in Groningen raises the question whether this intervention technique can additionally enhance the behaviour of masonry structures during seismic loading.

A masonry wall was experimentally tested in two configurations: a) a pre-damaged state, with simulated damage typical of imposed soil settlement, and b) a post-damaged and post-intervention state, this being the wall from the previous configuration after being tested to its maximum base shear and subsequently strengthened. Differences between the two configurations in terms of stiffness, peak force and prevalent damage patterns are discussed.

Accompanying the experimental campaign, results of finite element simulations of the strengthened wall are presented. The strengthened wall is simulated using non-linear macro-modelling techniques. The model accounts for the experimentally simulated damage as well as for the damage arising after the testing in the first configuration. The analysis results clarify and quantify the experimental observations on the strengthened wall, particularly as regards stress development and bond-slip in the reinforcement bars.

Based on the experimental and numerical results, the effectiveness of the intervention in restoring the strength of the wall and in preventing the re-emergence of major diagonal cracking is confirmed.

1 INTRODUCTION

1.1 State of the art and motivation

Induced seismicity is the term used for describing low-magnitude ground shaking caused by human activity. It is characterised by high frequency of incidence, potentially exceeding hundreds of events every year in a single location. Among the main human activities linked to the generation of induced seismicity events is gas extraction [1]. While these low-magnitude earthquakes typically do not pose a threat to the structural safety of buildings and infrastructure, they can gradually reduce the durability and aesthetic integrity of structures through the formation and accumulation of light damage.

Soil-subsidence and uplift are responsible for the formation of damage in structures. The difference in stiffness between the superstructure/foundation and the soil causes the induction of bending and shear strain in buildings, an effect known as soil-structure interaction [2]. Gas extraction, in addition to inducing seismicity, leads to soil subsidence over wide geographic areas. Masonry structures are particularly vulnerable to soil-structure interaction effects due to their high stiffness and low tensile strength.

Due to the presence of soft clay, sand and peat top-soils, the Dutch region of Groningen has continuously experienced soil subsidence. Over the preceding decades, repair measures have been employed against the effects of soil movement in historic and traditional masonry buildings. One such widely employed measure consists in the placement of stainless steel helical bars in bed joints repointed using a high strength mortar. Additional bars are placed across cracks formed in masonry through drilled pilot holes. In more recent times, gas extraction operations in the region have not only exacerbated soil subsidence, but have been the cause of induced seismicity. This combined action poses substantial risk to the durability of the masonry building stock in the region, including both vernacular and monumental structures [3]. The role of the embedded reinforcement bars in enhancing the seismic capacity of masonry buildings, a role for which it was not originally intended, has not been sufficiently studied.

The role of embedded steel or CFRP reinforcement in masonry has received some attention in the literature, in both experimental and numerical studies [4, 5, 6]. However, the role of bed joint reinforced repointing as the main means of strengthening has not been sufficiently investigated, particularly in full-scale structures.

1.2 Objectives

The main objective of the paper is the evaluation of the overall role of bed joint reinforced repointing for masonry walls on structural behaviour under in-plane earthquake loading. The conditions in Groningen require that the walls be tested in a combination of subsidence- and earthquake-induced loads. Further, the nature of induced seismicity requires that structural behaviour be evaluated for both low- and high-magnitude loading.

The strengthening technique is evaluated in terms of contribution to capacity and ductility. Additionally, the shift in failure mode during low- and high-magnitude loading is an important parameter to consider.

1.3 Methodology

The effectiveness of the strengthening was evaluated through preliminary experimental testing of masonry walls with dimensions and layout commonly encountered in Groningen. Two walls with a window opening and simulated damage were tested up to light damage. Subse-

quently, one of the walls was strengthened and re-subjected to the light damage loading protocol. Finally, both the unstrengthened and strengthened walls were tested up to failure.

Following the experimental testing, a numerical campaign was executed. The primary objective of the campaign was the simulation of the strengthened wall test. Different modelling techniques were employed in order to establish the influence of the modelling approach on the results.

This paper focuses on the numerical simulation of the in-plane testing of the strengthened wall. The experimental results of both the unstrengthened and strengthened walls are detailed in a separate work [7]

2 EXPERIMENTAL CAMPAIGN

2.1 Testing of constituent materials

The units were solid clay bricks measuring $210 \times 50 \times 100\ mm^3$ in length $\times$ height $\times$ width. The width of the walls is equal to the width of the units. These units are very typical in traditional clay-brick masonry construction in the Netherlands, including in Groningen, and feature a high compressive strength [8].

The construction mortar was an O-type lime cement mortar, with an expected compressive strength of $2.4\ N/mm^2$ at 28 days. While this mortar type is not typically recommended for load-bearing members in new construction, it offers a reasonable approximation of traditional mortars while simultaneously not requiring excessive curing time before developing a compressive strength sufficient for low-rise construction. The thickness of all mortar joints was $10\ mm$.

The properties of the units and mortar as determined experimentally are shown in Table 1.

Parameter	Symbol	Units	Average	Coefficient of variation
Unit compressive strength	$f_{c,u}$	N/mm^2	28.31	0.10
Mortar compressive strength	$f_{c,m}$	N/mm^2	3.59	0.09

Table 1: Results of masonry constituent material tests.

2.2 Testing of masonry composite

Masonry wallets were subjected to different mechanical tests for the determination of the properties of the masonry composite. Further, the mechanical properties of the unit-mortar interface were determined experimentally.

Compressive tests on the masonry composite were executed according to EN 1052-1 [9], both normal and perpendicular to the bed joints (vertical and horizontal directions).

The shear strength of the unit-mortar interface was characterised through triplet testing according to EN 1052-3 [10]. The tensile strength of the interface was determined through manually-operated bond-wrench testing according to EN 1052-5 [11].

The results of the masonry composite tests are summarised in Table 2.

2.3 Layout of masonry walls

The masonry wall samples measured $3070 \times 2690 \times 100\ mm^3$ in length $\times$ height $\times$ width, with an eccentric window opening measuring $780 \times 1510\ mm^2$ in length $\times$ height. The masonry was constructed in single-wythe running bond, with a concrete lintel constructed over the open-

Parameter	Symbol	Units	Average	Coeff. of variation
Horizontal compressive strength	$f_{c,x}$	N/mm^2	13.11	0.18
Vertical compressive strength	$f_{c,y}$	N/mm^2	12.93	0.07
Horizontal compressive fracture energy	$G_{c,x}$	N/mm	35.06	0.19
Vertical compressive fracture energy	$G_{c,y}$	N/mm	28.63	0.11
Horizontal Young's modulus	E_x	N/mm^2	3207	0.18
Vertical Young's modulus	E_y	N/mm^2	3190	0.24
Initial shear strength	f_{v0}	N/mm^2	0.13	-
Friction coefficient	μ	-	0.82	-
Shear fracture energy	G_v	N/mm	0.30	-
Flexural bond strength	f_w	N/mm^2	0.08	0.32
Flexural bond fracture energy	G_w	N/mm	0.0069	-
Density	ρ	kg/m^3	1708	0.07

Table 2: Material properties of masonry composite.

ing. The walls were constructed in a single day by an experienced mason. The samples were were constructed directly atop a steel HEB 300 beam and capped with a HEB 600 beam.

For the simulation of damage caused by soil settlement, thin plastic sheets were introduced at targeted locations between the units and the mortar, thus preventing the formation of the unit-mortar interface bond, but allowing the mortar to develop its compressive strength. This damage is designated as 'pre-damage' in this paper. It consists in diagonal cracks near the edges of the window, as would be formed from a sagging deformation towards the right of the wall.

The layout of the walls, along with the disposition of the pre- and post-damage, can be seen in Figure 1a.

2.4 Strengthening method and intervention materials

The strengthening method consists in two interventions: a) the embedment of horizontal helical bars in repointed bed joints and b) the insertion of diagonal helical bars in pilot holes across formed cracks, without grout or other anchoring measures.

The repair mortar used in this application is a strong cementitious intervention material that can be injected in mortar joints. Its expected compressive strength at 28 days is 45 N/mm^2. For the repointing of the bed joints, a 40 mm portion of the joint was removed from one face of the wall. Subsequently, helical bars were placed in the groove singly or in pairs and the groove was completely filled with the repair mortar. This intervention method introduces some eccentricity to the wall, since the bars are not placed centrally along the thickness of the wall and since the repair mortar, applied on a single face, is much stiffer than the construction mortar.

The helical bars are stainless steel grade ASTM 304, with a diameter of 6 mm. The steel has a yield strength of 215 N/mm^2 and a tensile strength of 505 N/mm^2. The bond-slip behaviour of the bars was investigated in two setups: a) in bars embedded in repair mortar for testing the behaviour of the bed joint reinforcement and b) in bars inserted vertically in masonry prisms for testing the behaviour of the diagonal reinforcement [12]. The test results were fitted to the piecewise Model Code 2010 bond-slip model [13]:

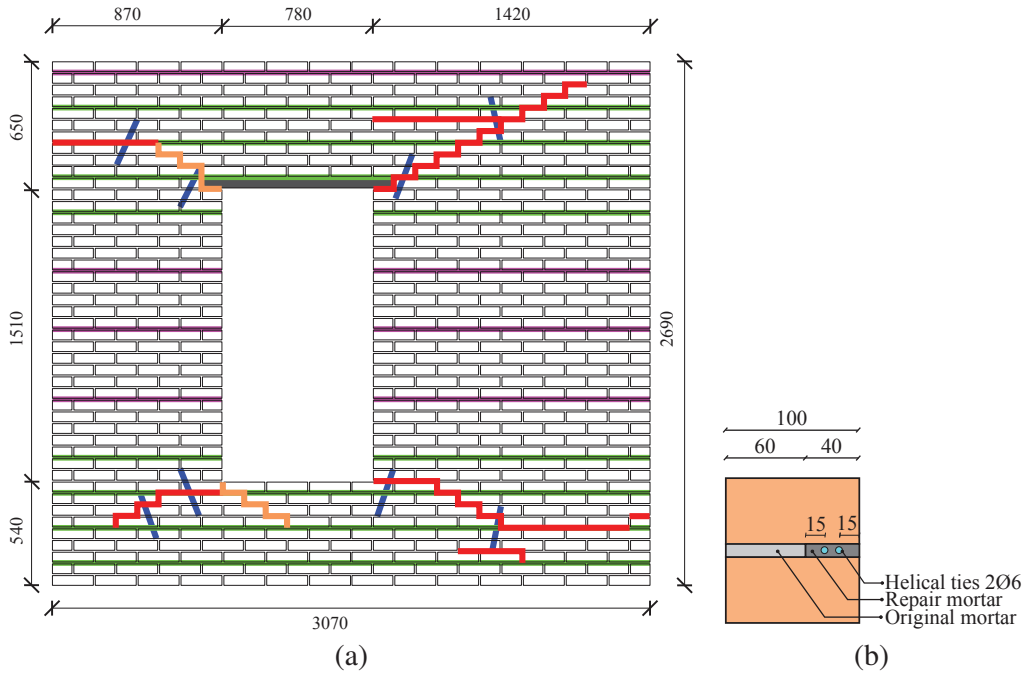

Figure 1: a) Layout of strengthened masonry wall. Pre-damage in orange, post-damage in red. Single bed joint bars in purple, double bed joint bars in green, diagonal anchors in blue. b) Cross-section of repointed joint. All dimensions in *mm*.

$$\tau_0(s) = \begin{cases} \tau_{max}\left(s/s_1\right)^a & \text{for} \quad 0 \leq s \leq s_1 \\ \tau_{max} & \text{for} \quad s_1 \leq s \leq s_2 \\ \tau_{max} - \left(\tau_{max} - \tau_f\right)\left(s - s_2\right)/\left(s_3 - s_2\right) & \text{for} \quad s_2 \leq s \leq s_3 \\ \tau_f & \text{for} \quad s_3 \leq s \end{cases} \tag{1}$$

where a is a numerical parameter controlling the shape of the initial branch, τ_{max} is the peak bond stress, τ_f is the residual bond stress and s_1, s_2 and s_3 are slip values determining the inflection points of the bond-slip curve. The value of s_1 is here considered as the elastic limit for the bond-slip. The experimentally determined bond-slip properties according to Eq. 1 are summarised in Table 3.

	s_1	s_2	s_3	τ_{max}	τ_f	a
	mm	mm	mm	N/mm^2	N/mm^2	-
Bed joint	5.0	110.0	120.0	2.0	0.05	0.7
Diagonal	20.0	45.0	50.0	1.3	0.05	0.7

Table 3: Numerical parameters for Model Code 2010 bond-slip model.

The properties of the repair materials are summarised in Table 4. The repair mortar was tested at 28 days and the properties of the bars are determined according to the properties of ASTM 304 stainless steel.

Material	Parameter	Symbol	Units	Average	Coeff. of variation
Repair mortar	Compressive strength	$f_{c,M}$	N/mm^2	46.42	0.09
	Flexural strength	$f_{b,M}$	N/mm^2	7.68	0.24
Helical bar	Young's modulus	E_s	N/mm^2	193000	-
	Yield strength	$f_{y,s}$	N/mm^2	215	-
	Tensile strength	$f_{t,s}$	N/mm^2	505	-

Table 4: Mechanical properties of repair materials.

2.5 Testing procedure for masonry walls

A vertical compressive load of $0.12\,N/mm^2$ was applied on the top beam. The testing setup allowed rotation of the top (cantilever configuration). The horizontal in-plane load was applied in displacement control through a horizontal actuator to the top steel beam. Digital image correlation and an arrangement of sensors were employed for monitoring the deformation and crack pattern of the walls.

Both walls were initially tested in their un-strengthened, pre-damaged state up to light damage. The damage due to this test, similar in pattern for both walls, was documented and designated as 'post-damage' and was concentrated at the mortar joints. These cracks propagate from the corners of the window, both as extensions of the pre-damage and in new locations, and propagated primarily in a diagonal direction. One wall was subsequently strengthened using the repair mortar and helical bars and diagonal ties. Finally, both walls were tested up to failure. The geometric layout of the bars is illustrated in Figure 1a, while a cross-section of a repointed bed joint can be seen in Figure 1b.

The loading protocol for in-plane shear-compression was designed in order to simulate the loading that may arise in regions were both soil settlement and induced seismicity are encountered [7]. Thus, the loading protocol for both tests was composed of three phases. In phase 1, low-magnitude repeated in-plane displacement was applied. In phase 2, low magnitude cyclic loading was applied. In phase 3 the target displacement per cycle was increased in magnitude up to failure of the wall. The loading protocol is detailed in Table 5. The net displacement refers to the displacement of the top beam with respect to an external reference point, excluding rotations of the setup and horizontal displacement of the bottom beam with respect to the external reference.

2.6 Experimental results

The results of the in-plane tests are illustrated in terms of force displacement graphs obtained in phase 3 in Figure 2. The eccentric placement of the window results in noticeable difference in the capacity and stiffness of the unstrengthened wall in the negative and positive direction. The unstrengthened wall presents substantial residual drift accumulation for negative displacement, whereas the residual drift is reduced in magnitude and oscillates according to the loading direction in the strengthened case.

Despite the wall having sustained substantial damage in the initial test, the strengthening technique not only restores the strength and stiffness of the wall, but modestly enhances these parameters. Similarly enhanced is the ductility of the wall, with limited reduction in the shear force after attaining its peak value. Further, the strengthening reduces the difference between the response in the negative and positive directions.

The crack patterns registered through digital image correlation for both the unstrengthened

Phase	Cycle	Runs	Net horizontal displacement	
				mm
1	C1	30	0.73	-
	C2	30	0.92	-
	C3	30	1.09	-
	C4	30	1.28	-
	C5	30	1.50	-
2	C6	30	0.73	-0.75
	C7	30	0.92	-0.96
	C8	30	1.13	-1.15
	C9	30	1.33	-1.37
	C10	30	1.53	-1.58
	C11	30	1.72	-1.77
	C12	30	1.93	-1.98
3	C13	4	2.48	-2.52
	C14	4	7.87	-7.91
	C15	2	13.28	-13.29
	C16	2	26.76	-26.79
	C17	2	40.25	-40.30
	C18	2	53.77	-53.80
	C19	2	67.26	-67.28
	C20	2	80.76	-63.31

Table 5: Loading protocol for the in-plane shear-compression test.

and strengthened walls are illustrated in Figure 2. In the unstrengthened wall the diagonal cracking around the window is prevalent. The presence of the bars in the strengthened wall produces a shift in the arrangement of the crack pattern. The bed joint reinforcement prevents for the most part the diagonal cracks from propagating, resulting in the formation of more pronounced horizontal cracks. These cracks are well-defined at the top of the two piers, but are more distributed at the base of the piers. Damage in the spandrel is significantly limited compared to the unstrengthened case. Both piers in both tests are generally undamaged due to the predominance of rocking in their response. Toe crushing was not extensive due to the low vertical load.

3 NUMERICAL SIMULATION OF STRENGTHENED WALL

3.1 Modelling approach

The modelling campaign presented here focuses on the strengthened wall. Analyses of the unstrengthened wall, with the absence of pre-damage, have been presented in a previous work [14].

For the simulation of the in-plane experiment, a finite element macro-modelling approach is adopted in this paper. In this approach, the masonry composite is modelled as a plane stress orthotropic continuum, with no distinction between units and mortar in the analysis domain. The mean edge length of the finite element mesh was 30 *mm*. Each cycle of the loading protocol was executed once. A regular Newton-Raphson scheme was employed for the iterations and an energy norm of 0.1% was used as a convergence criterion at each load step.

The finite element model was constructed and analysed using the DIANA finite element

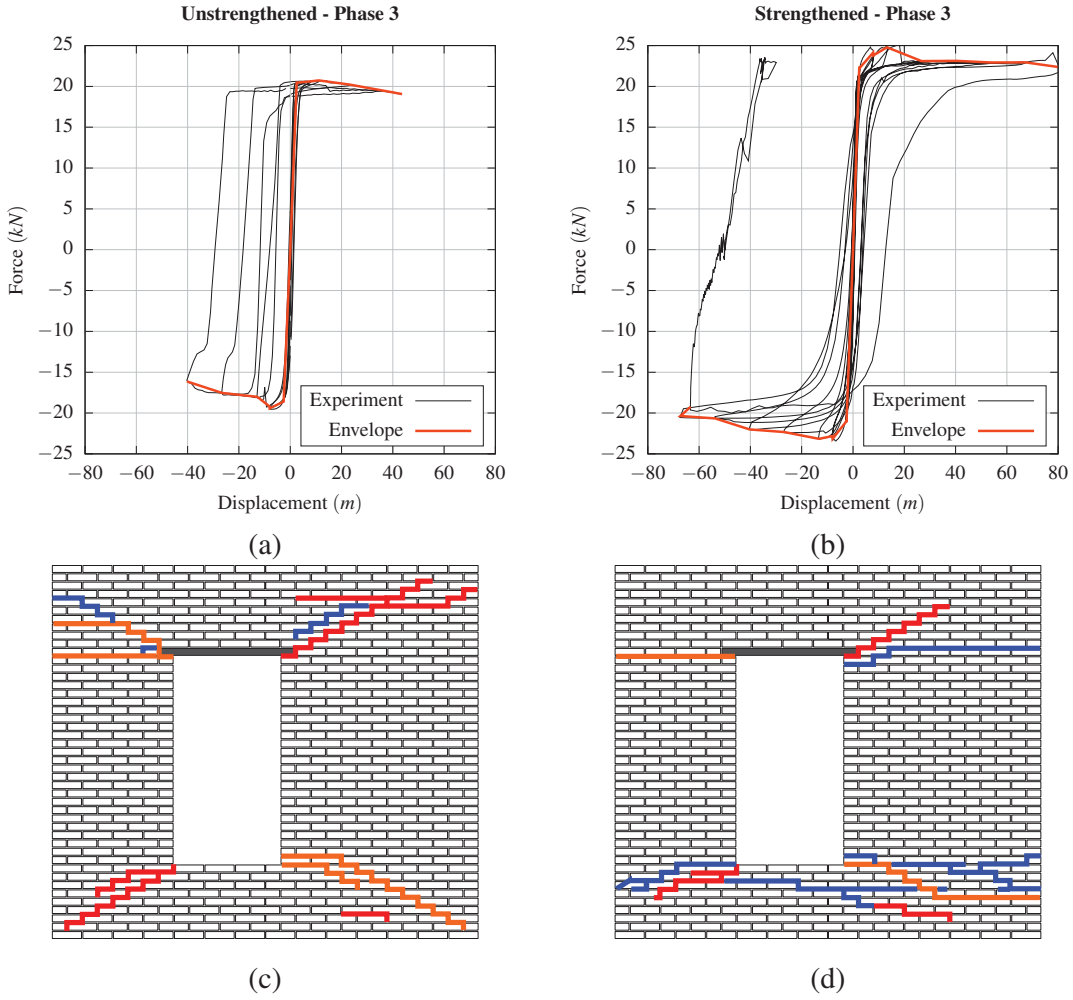

Figure 2: Force-displacement graphs for phase 3: a) unstrengthened wall and b) strengthened wall. Experimentally obtained damage patterns for: c) unstrengthened wall and d) strengthened wall. Damage arising in phase 1 (orange), in phase 2 (red) and in phase 3 (blue).

program. Material non-linearity was modelled using the Engineering Masonry Model, jointly developed by TU Delft and DIANA FEA [15]. Within an anisotropic total strain context, the model accounts for the compressive, shear and tensile failure of the masonry composite.

The tensile strength of the masonry composite in two orthogonal in-plane directions is calculated as a function of the masonry bond, unit-mortar bond strength, friction angle and shear strength.

In the direction normal to the continuous bed joints (vertical), the tensile strength of masonry is determined at the load of first cracking during the bond strength test, empirically equal to:

$$f_{t,y} = \frac{2}{3} f_w \tag{2}$$

In the direction parallel to the bed joints (horizontal), the tensile strength of masonry is equal to:

$$f_{t,x} = \tau_{max} / \tan(\alpha) \tag{3}$$

where α is the angle between the staircase crack and the bed joint (here equal to 0.50 rad) and τ_{max} is equal to:

$$\tau_{max} = \max\left[0, f_{v0} - \sigma_y \mu\right] \tag{4}$$

where σ_y is the vertical stress, compression being negative. Diagonal staircase cracking, defined as the opening of a crack at an angle of α from the horizontal, is evaluated against the diagonal tensile strength, calculated as:

$$f_{t,a} = \frac{f_{t,x} f_{t,y}}{f_{t,x}^2 \sin^2\left(\frac{\pi}{2} - \alpha\right) + f_{t,y}^2 \cos^2\left(\frac{\pi}{2} - \alpha\right)} \tag{5}$$

The reinforcement bars were modelled as truss elements embedded in the plane stress elements. Their bond-slip behaviour is modelled by considering a uniaxial constitutive relation between slip and bond stress according to Eq. 1. Yielding of the bars is also considered with a uniaxial constitutive relation between axial strain and stress according to the properties of ASTM 304 stainless steel. The material properties as summarised in Table 2 and Table 3 were used as input for the model without further calibration.

To model the pre- and post-damage, reduced strength and stiffness were assigned to the damaged areas of the masonry. The compressive strength was left unchanged due to the damage having been caused by opening of the unit-mortar interface. The tensile and shear strength, as well as the tensile and shear fracture energy, were reduced to zero in order to account for the artificial absence of bond in the pre-damage and the loss of interface cohesion in the post-damage due to crack opening. The Young's modulus was reduced by 50% in all damaged locations.

The top steel beam was modelled as an elastic beam element in perfect bond with the masonry wall. The model was clamped at the base and unrestrained at the top. Out-of-plane effects that may arise due to the eccentricity of the reinforcement were not considered in the model.

4 NUMERICAL ANALYSIS RESULTS

The numerical force-displacement curve for phases 1 and 2, in comparison with the experimentally derived curve, is presented in Figure 3. The stiffness of the structure is approximated well. The peak force is overestimated by 20% in the positive direction, but predicted with good accuracy in the negative direction. The hysteresis loops are also better approximated in the negative direction.

The numerically obtained crack patterns are shown in Figure 4 at the instances of peak negative and positive applied displacement. The cracking pattern matches the experimentally obtained damage to a significant extent, with the exception of the re-opening of the diagonal crack at the upper left corner of the window for positive displacement instead of the formation of a new horizontal crack propagating towards the edge of the wall. The difference in the crack pattern for positive displacement is possibly linked to the overestimation of the peak force in that loading direction. It is interesting to note that this horizontal crack was formed in the unstrengthened wall during phase 1 but was not formed in the wall that was eventually strengthened.

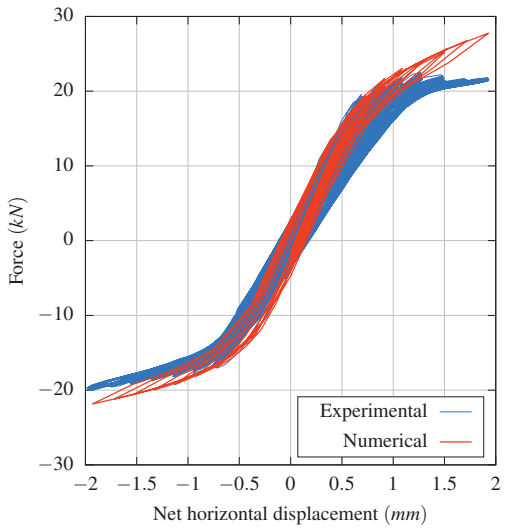

Figure 3: Comparison of experimental with numerically-derived force-displacement curve for phase 2.

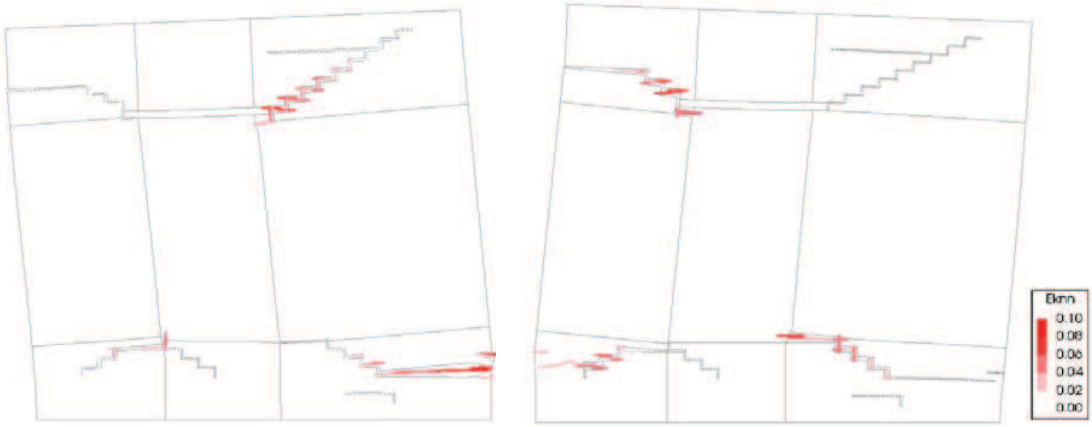

(a) (b)

Figure 4: Numerically obtained crack patterns, as crack strain vectors parallel to the crack in red, for phase 2 at: a) peak negative displacement ($-1.98\ mm$) and b) peak positive displacement ($1.93\ mm$).

The bed joint reinforcement, being oriented in parallel with the main direction of cracking, did not register any substantial slipping. The maximum axial stress borne by the bed joint bars was $53.2\ N/mm^2$ well below the yield strength ($215\ N/mm^2$). The maximum slip of the diagonal anchors was roughly $0.26\ mm$, while the maximum axial stress was limited to $1.5\ N/mm^2$.

The numerical force-displacement curve for phase 3, in comparison with the experimentally derived curve, is presented in Figure 5. The stiffness of the structure is well approximated, as is the capacity in the negative direction. As in the simulation of the previous phase, an overestimation of the capacity in the positive direction was obtained, but this overestimation is much reduced in this phase. The hysteresis cycles are well approximated up to a displacement of $20\ mm$ and $40\ mm$ in the positive and negative directions respectively. The residual resistance of the wall in the positive direction is very well approximated and is slightly overestimated in

the negative direction.

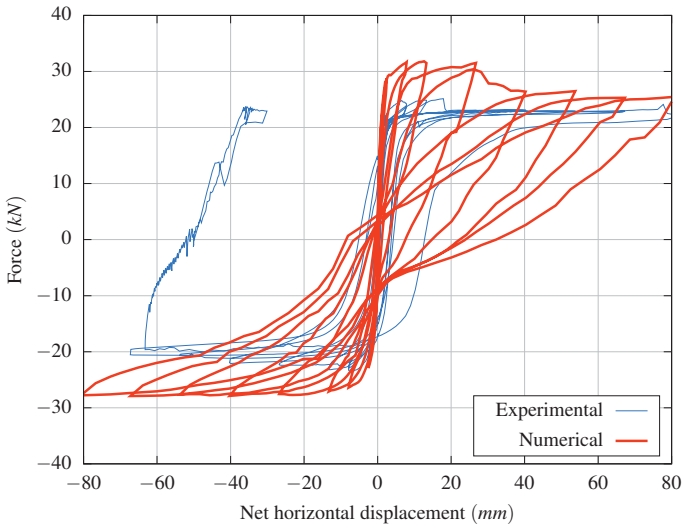

Figure 5: Comparison of experimental with numerically-derived force-displacement curves for phase 3.

The cracking pattern obtained numerically for phase 3 is shown in Figure 6. In the negative loading direction the network of mostly horizontal cracks formed at the lower right portion of the base of the wall is reproduced numerically. The cracks at the lower left of the window are partially reproduced, while the horizontal crack starting at the upper right edge of the window is partially reproduced in the simulation. For applied positive displacement, the horizontal crack at the upper left edge of the window propagates to a greater degree and is in better agreement with the experimental results. The length of the crushed toe is negligible due to the low ratio of applied vertical stress over the compressive strength.

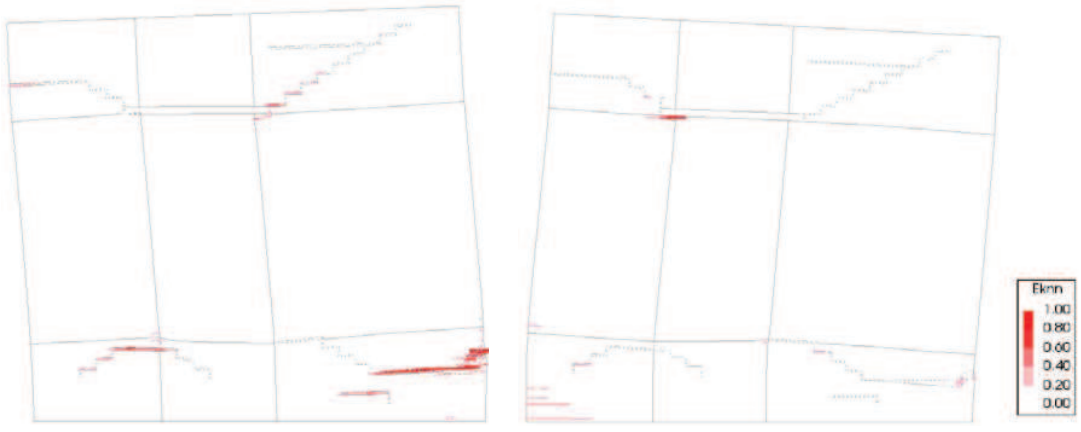

(a) (b)

Figure 6: Numerically obtained crack patterns, as crack strain vectors parallel to the crack in red, for phase 3 at: a) peak negative displacement and b) peak positive displacement.

Similarly to the results obtained in phase 1 and 2, slipping in the horizontal bars is negligible.

However, the peak axial stress registered at the lower right of the opening for maximum applied horizontal displacement was 239.1 N/mm^2, which is slightly higher than the yield strength. The maximum slip of the diagonal anchors was 8.2 *mm* and the maximum axial stress 21.9 N/mm^2.

The behaviour of the reinforcement at key locations on the structure is detailed in Figure 7. The axial stress of the bed joint reinforcement follows a generally linear correlation with the applied net displacement, up to an applied displacement of 40 *mm*. For higher applied displacement the peak axial stress hovers at a plateau of roughly 230 N/mm^2, which is higher than the yield stress of 215 N/mm^2. The bond-slip at the diagonal bars above the window opening remain below than 1 *mm* for an applied displacement lower than 7.91 *mm*. For higher levels of applied displacement, the bond-slip obtained at the peak of the load cycle increases linearly with the net horizontal displacement.

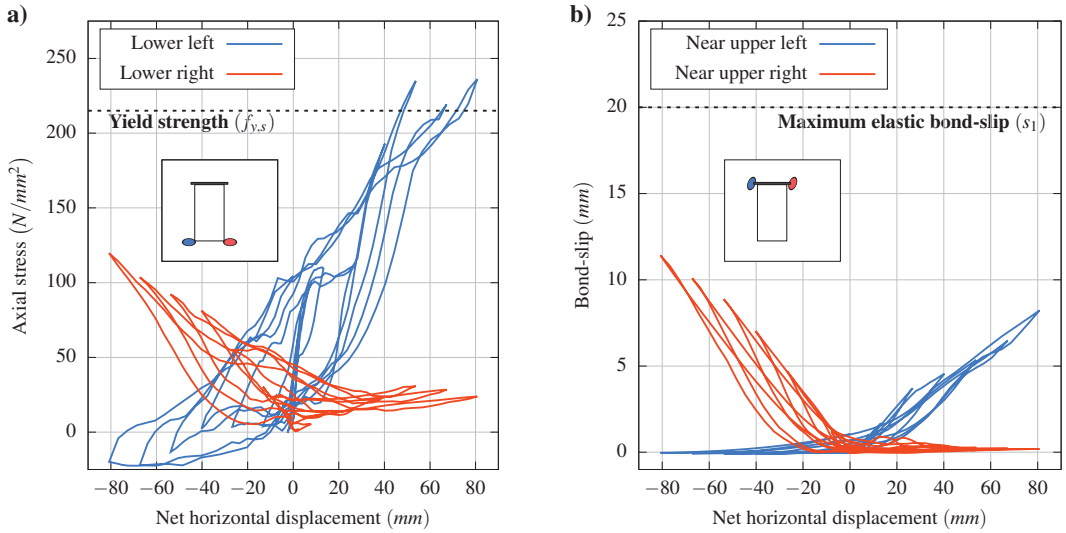

Figure 7: Numerically calculated behaviour of reinforcement during phase 3: a) axial stresses at bed joint reinforcement bars below the window opening and b) bond-slip of diagonal anchors above window opening. Locations of measurement indicated in colour-coded wall drawing insets.

It is generally concluded that the diagonal anchors, due to the low stiffness of their bond with the masonry, develop very low axial stresses and exhibit substantial bond-slip. Increasing the bond with the masonry through an enhancement of the mechanical anchoring of these bars could potentially increase their contribution to the behaviour of the strengthened wall. Conversely, the bed joint bars, which feature a stronger bond with the repair mortar, contribute more substantially to the response of the wall through the restraint of diagonal crack propagation. Bond-slip is negligible but yielding occurs below the window opening for high applied net displacement. Due to their orientation, these bars do not contribute to the rocking mode capacity of the piers, but are nevertheless effective in reducing crack propagation, particularly in the spandrel.

Overall, without resorting to any undue calibration of material parameters, the numerical effort is able to reproduce the main characteristics of the response registered in the experiments. This renders the numerical results a valuable tool in the assessment of the performance of the reinforcement, direct measurements of which were not possible to be acquired during the experiments. Finally, the capture of the main characteristics of the response through the model paves the way for application in larger and more complex cases.

5 CONCLUSIONS

The performance of bed joint reinforced repointing as employed for masonry structures in the Groningen region of the Netherlands was investigated. A masonry structure subjected to settlement-induced damage, followed by in-plane seismic loading was experimentally tested. The structure was strengthened using a technique widely employed in practice but lacking in rigorous experimental validation.

The reinforcement was experimentally shown to provide a modest increase to the in-plane stiffness and force capacity of masonry walls, in addition to a substantial increase in displacement capacity. This is accomplished despite the presence of damage induced by settlement and prior seismic loading. The strengthening is shown to prevent new diagonal cracks from forming in the spandrels, reduces the obtained crack width and reduces the crack propagation length.

The experimental tests were simulated numerically for assisting in the interpretation of the experimental results and for the investigation of the performance of the bed joint reinforcement and anchors. The numerical reproduction of the tests highlights crucial aspects in the performance of the reinforcement. Minimal bond-slip occurs and high axial stresses are developed in the bed joint bars. Conversely, the diagonal anchors exhibit substantial slipping and low axial stresses. It is therefore concluded that the contribution of the bed joint reinforcement is more substantial than that of the anchors.

ACKNOWLEDGEMENTS

This research was funded by the Rijksdienst voor het Cultureel Erfgoed (RCE), part of the Ministerie van Onderwijs, Cultuur en Wetenschap (OCW), subsidy No. MS-2018-189, which is gratefully acknowledged.

REFERENCES

[1] G. Foulger, MP. Wilson, JG. Gluyas, BR. Julian, RJ. Davies. Global review of human-induced earthquakes. *Earth-Science Reviews*, **178**, 438–514, 2018.

[2] M. Son, EJ. Cording. Evaluation of Building Stiffness for Building Response Analysis to Excavation-Induced Ground Movements. *Journal of Geotechnical and Geoenvironmental Engineering*, **133**, 995–1002, 2007.

[3] P. Van Staalduinen, K. T, JG. Rots. Onderzoek naar de oorzaken van bouwkundige schade in Groningen Methodologie en case studies ter duiding van de oorzaken. Report no. CM-2018-01, Delft University of Technology, 2018.

[4] VG. Haach, G. Vasconcelos, P. Lourenço. Parametrical study of masonry walls subjected to in-plane loading through numerical modeling. *Engineering Structures*, **33**, 1377–1389, 2011.

[5] N. Ismail, RB. Petersen, MJ. Masia, JM. Ingham. Diagonal shear behaviour of unreinforced masonry wallettes strengthened using twisted steel bars. *Construction and Building Materials*, **25**, 4386–4393, 2011.

[6] RB. Petersen, MJ. Masia, R. Seracino. In-Plane Shear Behavior of Masonry Panels Strengthened with NSM CFRP Strips. I: Experimental Investigation. *Journal of Composites for Construction*, **14**, 754–763, 2010.

[7] L. Licciardello, JG. Rots, R. Esposito. Performance of unreinforced masonry strengthened with bed joint reinforced repointing. In *12th International Conference on Structural Analysis of Historical Constructions, Barcelona, Spain*, 2020.

[8] S. Jafari, JG. Rots, R. Esposito, F. Messali. Characterizing the Material Properties of Dutch Unreinforced Masonry. *Procedia Engineering*, **193**, 250–257, 2017.

[9] CEN. *EN 1052-1 - Methods of test for masonry - Part 1: Determination of compressive strength*. 1999.

[10] CEN. *EN 1052-3 - Methods of test for masonry - Part 3: Determination of initial shear strength*. 2002.

[11] CEN. *EN 1052-5 - Methods of test for masonry - Determination of bond strength by the bond wrench method*. 2005.

[12] L. Licciardelo, R. Esposito. Experimental study on unreinforced masonry strengthened with bed joint reinforcement. Report no. CM1B07-2, Delft University of Technology, 2019.

[13] Federátion Internationale du Béton. *The fib Model Code for Concrete Structures 2010*. Wiley and Sons, 2013.

[14] PA. Korswagen, M. Longo, E. Meulman, JG. Rots. Crack initiation and propagation in unreinforced masonry specimens subjected to repeated in-plane loading during light damage. *Bulletin of Earthquake Engineering*, **17**, 4651–4687, 2019.

[15] JG. Rots, F. Messali, R. Esposito, S. Jafari, V. Mariani. Computational modelling of masonry with a view to Groningen induced seismicity. In *Structural Analysis of Historical Constructions: Anamnesis, diagnosis, therapy, controls - Proceedings of the 10th International Conference on Structural Analysis of Historical Constructions, SAHC 2016*, 227–238, 2016.